Snow depth mapping in high alpine catchments using digital photogrammetry

Y. Bühler[1], M. Marty[3], L. Egli[2], J. Veitinger[1,4], T. Jonas[1], P. Thee[3] and C. Ginzler[3]

[1]{WSL Institute for Snow and Avalanche Research SLF, Davos, Switzerland}

[2]{World Radiation Center PMOD WRC, Davos, Switzerland}

[3]{Swiss Federal Institute for Forest, Snow and Landscape Research WSL, Birmensdorf, Switzerland}

[4]{Department of Geography, University of Zurich, Zurich, Switzerland}

Correspondence to: Y. Bühler (buehler@slf.ch)

Abstract

Information on snow depth and its spatial distribution is crucial for numerous applications in snow and avalanche research as well as in hydrology and ecology. Today snow depth distributions are usually estimated using point measurements performed by automated weather stations and observers in the field combined with interpolation algorithms. However, these methodologies are not able to capture the high spatial variability of the snow depth distribution present in alpine terrain. Continuous and accurate snow depth mapping has been successfully performed using laser scanning but this method can only cover limited areas and is expensive. We use the airborne ADS80 opto-electronic scanner, acquiring stereo-imagery with 0.25 m spatial resolution to derive digital surface models (DSMs) of winter and summer terrains in the neighborhood of Davos, Switzerland. The DSMs are generated using photogrammetric image correlation techniques based on the multispectral nadir and backward looking sensor data. We compare these products with the following independent datasets acquired simultaneously: a) manually measured snow depth plots b) differential Global Navigation Satellite System (dGNSS) points c) Terrestrial Laser Scanning (TLS) and d) Ground Penetrating Radar (GPR) datasets, to assess the accuracy of the photogrammetric products. We demonstrate that the presented method can be used to map snow depth at two-meter resolution with a vertical depth accuracy of ±30 cm (root mean square error) in the

complex topography of the Alps. The presented snow depth maps have an average accuracy that is better than 15% compared to the average snow depth of 2.2 m over the entire test site.

1 Introduction

Snow is an important resource in alpine regions not only for tourism (e.g. Elsasser and Bürki, 2002; Nöthiger and Elsasser, 2004; Rixen et al., 2011) but also for hydropower generation and water supply (e.g. Marty, 2008; Farinotti et al., 2012) and ecological aspects of the local mountain flora and fauna (e.g. Wipf et al., 2009). Snow is also important in the context of natural hazard prevention, such as avalanches or flood forecast in spring and early summer for the valleys downstream. For the latter it has been shown that the snow distribution at the winter maximum before the beginning of the melting period strongly determines the temporal evolution of the remaining snow resources and - if converted to snow water equivalent (Jonas et al. 2010) - the potential melt water run-off during the melting period (Egli et al. 2011). Several studies reported a very high spatial variability of snow depth and other snow pack parameters at different spatial scales in mountainous regions. (e.g. Elder et al. 1991; Schweizer et al. 2008, Lehning et al. 2008, Grünewald et al. 2010, Egli, 2011). This high variation of snow cover distribution at very small scales requires a high spatial resolution of snow samples to measure different parameters of the snow pack such as e.g. the areal mean snow depth on complex Alpine topography and the temporal evolution of snow covered areas during melt with high areal representativeness and low absolute uncertainty. In other words, snow pack monitoring in Alpine terrain requires an area wide observation with a large number of snow depth point measurements distributed over the area of interest.

Currently, in the Swiss Alpine region snow depth is measured at specific locations by automated weather stations or observers in the field, while both observations are restricted to flat sites exhibiting a rather homogeneous snow cover (Bründl et al. 2004; Egli 2008). These flat field point measurements are assumed to represent snow cover characteristics for a larger area around the stations and are therefore interpolated over large distances and are combined with snow cover information from optical satellites (Foppa et al., 2007). This method is unable to capture the small-scale variability of snow depth. Investigations on the representativeness of point snow depth measurements on snow depth for entire catchments are sparse (Grünewald and Lehning 2014).

Remote sensing instruments have been used for snow related studies since such data became available (e.g. Rango and Itten, 1976; Dozier 1984, Hall and Martinec, 1985). A very common parameter measured by remote sensing instruments is snow-covered area (SCA). Operational products on global scale such as Modis Snow-cover Products (Hall et al., 2002) or GlobSnow (Koetz et al., 2008) are widely used today (Frei et al., 2012). For example Dozier (1989), Nolin and Dozier (1993), Fily et al. (1997) and Dozier et al. (2009) published investigations on snow grain size with finer spatial resolution on regional scale. Snow depth and Snow Water Equivalent (SWE) has been assessed using passive microwave sensors (e.g. Ulaby and Stiles, 1980; Chang et al. 1982; Pulliainen, 2006). However due to the coarse spatial resolution of these sensors (25 km), the results do not display small-scale snow cover characteristics of alpine catchments. Active microwave sensors use much smaller wavelength (mm to cm) and achieve finer spatial resolutions up to 20 m (e.g. Schanda et al. 1983; Shi and Dozier 2000; Rott and Nagler 1994). However this method is limited to dry snowpacks and faces problems in steep high-alpine terrain (Buchroithner 1995). Nolin (2011) and Dietz et al. (2012) give an overview on recent advances in remote sensing of snow.

Terrestrial Laser Scanning (TLS) was previously used to derive spatially continuous snow depth (Prokop, 2008; Gruenewald et al., 2010). Even though the accuracy of such measurements is very good (usually better than 0.1 m, depending on laser footprint and distance from sensor), large-scale catchments such as the Dischma valley (Figure 1) cannot be covered completely. Data acquisition with TLS is time/manpower consuming and only possible at easily accessible spots under fair conditions (avalanche situation, weather) for areas within line-of-sight from the measurement location. This results in limited coverage and many data gaps e.g. behind bumps. Airborne laser scanning (ALS) from helicopters or airplanes can cover larger areas in shorter time also under difficult avalanche danger situations. Recent studies demonstrate that accurate mapping of snow depth is possible (Deems et al. 2013, Mevold and Skaugen 2013). However, the costs to cover larger areas are still high (Bühler et al., 2012) and over-flights are, as with digital photogrammetry, restricted to fair weather conditions.

Previous attempts to map snow depth using scanned aerial imagery were already made 50 years ago (Smith et al. 1967) and the topic was investigated in detail by Cline (1993 and 1994). However their results suffer from image saturation and insufficient reference data leading them to the conclusion that photogrammetry has big potential but is not yet accurate enough for large scale snow depth mapping. Ledwith and Lunden (2010) used scanned aerial imagery to derive digital elevation models over glaciated and snow-covered areas in Norway.

They report a mean accuracy of 2.8 m in comparison with differential Global Navigation Satellite System (dGNSS) transects, which is clearly too low for meaningful snow depth mapping in alpine regions. Lee et al. (2008) used a DMC digital frame camera to cover an area of approximately 2.3 km^2 with a very high mean Ground Sampling Distance (GSD) of 0.08 m. The reported mean differences compared to dGNSS measurements are approximately 0.15 m stressing the big potential of digital photogrammetry for accurate snow depth mapping. However no snow depth mapping has been performed and compared to different reference data sets, covering larger areas.

In this investigation we apply digital photogrammetry based on high spatial resolution aerial imagery (0.25 m) to calculate digital surface models (DSM) of winter and summer terrain. Traditional photogrammetry using analogue aerial imagery and 8bit digital sensors faced problems over snow-covered areas mainly due to saturation and the homogenous surface (Kraus, 2004). Modern digital sensors can acquire data with 12bit radiometric resolution to overcome these limitations. We calculate spatially continuous snow depth maps using the summer and winter DSMs for two test sites near Davos, Switzerland (145 km^2 in total). This technology is much more economical to cover large areas than ALS or TLS but still has an acceptable spatial resolution to map the small-scale spatial variability. To assess the accuracy of our results we compare the calculated snow depths to hand measurements, dGNSS points, TLS measurements and GPR transects acquired simultaneously with the aerial imagery.

2 Test sites Wannengrat and Dischma, Davos, Switzerland

The two areas covered by the ADS80 sensor on a Pilatus Porter airplane are located close to the winter sport resort Davos in the eastern part of Switzerland (Figure 1).

The Wannengrat test site is located to the north of Davos and covers an area of approximately 3.5 x 7.5 km (26.25 km^2). The valley bottom is about 1500 m a.s.l., the highest peaks reach up to 2780 m a.s.l (Amselflue at the southwestern part of the test site). The large ski resort Davos-Parsenn is located at the northeastern edge of the test site. The covered mountain chain is characterized by high-alpine meadows, rock faces and scree covered areas. The area below 2000 m a.s.l. is covered by sparse- and from ca. 1800 m a.s.l. by dense forest. The Wannengrat area is used as test site for various research project at the WSL Institute for Snow and Avalanche research SLF mainly because of the very good accessibility from Davos even if the avalanche danger level is considerable. We collected hand measured snow depth plots, dGNSS points and TLS datasets close to the Wannengrat peak as reference datasets (see chapter 3.2) on the day of the ADS80 data acquisition.

The Dischma test site is a high-alpine valley branching from the main valley of Davos (1500 m a.s.l.) in southeastern direction up to 2000 m a.s.l. at the end of the valley covering an area of ca. 7 x 17 km (119 km^2) containing the complete catchment of the Dischma creek where several hydrological studies have been performed (Bavay et al. 2009). The peaks surrounding this catchment reach up to 3130 m a.s.l. (Piz Grialetsch). Forest covers the lower part of the valley up to 2000 m a.s.l. The southeastern two thirds of the valley are completely forest free. We collected GPR snow depth measurements at the valley bottom in the northwestern part of the test site as reference data on the day of the ADS80 data acquisition. Because the central flight strip at the valley bottom was corrupted in the summer 2010 dataset, resulting in a low quality summer DSM, we repeated the flight in summer 2013.

3 Sensors and datasets

To measure spatially continuous snow depth and to validate these measurements we use independent state-of-the-art technologies. It is a difficult task to measure multiple, spatially widely distributed snow depths in high-alpine areas within a short timespan. Several teams were deployed in the field on the day of the ADS80 data acquisition, guaranteeing a small temporal offset to the ADS80 imagery because snow depth can change very quickly under spring conditions.

3.1 Airborne opto-electronic Scanner ADS80

Two optoelectronic line scanner datasets were acquired with the ADS80-SH52 sensor. The acquisition of the summer images was realized on August 12th 2010 (Wannengrat) and September 3rd 2013 (Dischma). Winter imagery of the snow-covered sites was acquired on March 20th 2012 (close to the maximum snow cover, peak of winter). The covered area consists of 12 overlapping image strips (approx. 70% overlap across track) flown during approximately 90 minutes at an elevation of approximately 4000 m a.s.l. (1500 m above mean ground elevation). The mean Ground Sampling Distance (GSD) of the imagery is 0.25 m, limited through the minimal flying height for high alpine terrain (Buehler et al. 2012). The ADS80 scanner acquires simultaneously four spectral bands (red: 604 – 664 nm, green: 553 – 587 nm, blue: 420 - 492, near infrared: 833 – 920 nm) and a panchromatic band (465 – 676 nm) with a radiometric resolution of 12 bits and two viewing angles (nadir and 16°

backward,). The nadir and forward-looking panchromatic bands were not used due to saturation issues caused by the broader sensitivity of these bands. GNSS/IMU supported orientation of the image strips supplemented by the use of ground control points achieve a horizontal accuracy (x,y) of 1-2 GSD (0.25-0.5 m). The sources of the used ground control points are a combination of GNSS ground surveys and already existing oriented stereo images (with unknown absolute accuracy). We tried to distribute the GCPs regularly, however they are denser at the lower altitudes. We applied between 11 and 33 ground control points per acquisition date showing residuals of 3 to 21 cm in x, 4 to 17 cm in y and 10 to 33 cm in z direction. The ADS sensor was successfully used to detect avalanche deposits in the area of Davos (Bühler et al. 2009). Sandau (2010) gives more detailed information on the Leica ADS opto-electronic scanner.

3.2 Reference datasets

3.2.1 Manual snow depth measurements

Simultaneous with the ADS80 data acquisition, a field team acquired manual snow depth measurements using a 3.2 m avalanche probe at 15 different plot locations within the test site Wannengrat. A plot consists of 5 by 5 probe measurements with a distance of 2 m between points (Figure 2a) resulting in 375 single probe measurements localized using dGNSS of the corner points. Because snow depth can vary substantially within the distance of some decimeters if there is e.g. a rock at the surface (Lopez-Moreno et al. 2006), we use the average snow depth and the standard deviation to compare it to the corresponding ADS80 snow depth values within this 10 by 10 m area (Figure 2b). The acquisition of field measurements is very challenging because the terrain is steep and the human mobility is limited. The avalanche danger for wet snow avalanches rises quickly during the day due to sunny spring weather conditions, limiting the time the field team can move within the test sites. Therefore the number of performed field measurements at 15 plots distributed over an area of 1 by 1.5 km is close to the possible maximum that can be obtained with the number of workers participating in the experiment. Because this number is in our opinion not sufficient to assess the potential of the proposed method, we apply further reference data sets.

3.2.2 Differential Global Navigation Satellite System (dGNSS) measurements

During ADS80 data acquisition on 20th March 2012, 137 dGNSS points were measured with the Leica GPS 1200 device in the test site Wannengrat (Figure 2a). The points were measured with real-time correction using the virtual reference station of the swisstopo AGNES network in Davos. The surveyed points show a horizontal accuracy better than 1 cm (1standard deviation) and a vertical accuracy better than 2 cm (1 standard deviation) respectively. Measured points represent the top of the snow cover in m a. s. l.

3.2.3 Terrestrial Laser Scanning (TLS)

In the last decade, terrestrial laser scanning has been increasingly applied for continuous snow depth mapping (e.g. Deems 2013, Schirmer et al. 2011, Prokop 2008; Prokop et al. 2008). To calculate snow depth, an elevation model of the bare ground and another one of the snow covered winter surface is produced. Snow depth is then obtained by subtracting the two surfaces from each other. In this study, we use the Riegl LPM-321 device operating at 905nm. This device has been prooven to accurately measure snow depth in alpine terrain (Prokop 2008, Prokop et al. 2008). Grünewald et. al 2010 compared TLS measurements to Tachymeter measurements and found a mean vertical deviation of 4 cm with a standard deviation of 5 cm at a distance of 250 m using the LPM-321. To assure the quality of the laser scans, we additionally performed reproducibility tests. A laser scan acquired in a coarse resolution (3 points per m^2 at a distance of 300 m) was compared with the full resolution acquisition (8 points per m^2 at a distance of 300 m). This allows detecting misalignments between the two datasets due to an instable scan setup (unstable tripod, wind influence, etc). Scans which showed a mean difference larger than 10 cm were excluded. The upper end of the Steintaelli was scanned once in summer 2011 and a second time on March 20th 2012 during the ADS80 data acquisition (Figure 2c). Fixed installed reflector points were used to match the summer and winter TLS datasets.

3.2.4 Ground Penetrating Radar (GPR)

GPR data were collected using a MALÅ ProEx system configured for synchronous measurements with four pairs of separable shielded 400 MHz antennas. The antennas were set up as a common-mid-point (CMP) array with separation distances of 0.31, 0.95, 1.6, and 2.8 m respectively. The GPR antennas were mounted on two pulkas, which were rigidly connected to one another to guarantee fix relative antenna positions throughout the measurements. This assembly was pulled along a transect of 4.8 km length. After initial stacking of four individual traces, data were recorded every 0.5 seconds, which resulted on average in one record every 30 centimeters along the transect. GPS coordinates were taken every second along the transect using an onboard GPS receiver as well as an external Trimble GeoExplorer 6000 dGNSS system. GPS data were slightly smoothed before associating them with the GPR data records. Snow depth data were obtained using standard CMP analysis procedures partly involving the commercial software package ReflexW 7.0 (Sandmeier, 2013). Along the GPR transect we obtained 130 manual snow depth readings. These data were used for cross validation of the GPR data. Concurrent GPR and manual snow depth ranged from 0.76 to 2.70 m. Correlation between both data sets resulted in an R^2 of 0.96 and a RMSE of 0.07 m.

4 Generation of summer and winter digital surface models

For DSM generation we use the "Adaptive Automatic Terrain Extraction" (ATE) as part of the SOCETSET software version 5.4.1 from BAE SYSTEMS. The software implements an area-based algorithm calculating similarity measures with a two-dimensional cross-correlation approach. ATE has no need for user input on specific image matching strategies and parameters as a function of terrain type. ATE uses an "inference engine" which adaptively generates image matching parameters depending on facts such as terrain type, signal power, flying height or X and Y parallax. A user given post spacing distance is used to control image correlation spacing (e.g. 2 m), hence cross correlation is not calculated for every image pixel (Zhang and Miller, 1997). We use the green, red and near infrared bands of the sensor as input. The near infrared band absorbs a larger part of the incoming radiation over snow and the reflected signal is sensitive to grain size variation within short distances (Bühler et al. 2015). This improves the performance of the ATE point-matching algorithm in particular over old snow covers, not recently covered by new snow.

ATE SocetSet gave the best results regarding blunders and completeness. We also tested NGATE from SocetSet, XPro5.2 from Leica and MatchT5.1 from Inpho. XPro and MatchT use semi global matching techniques (SGM) for image correlation. Although this is the state-of the-art method for dense image matching (especially in urban areas with a very high image overlap) the results on snow surface was comparable or even worse to ATE SocetSet. MatchT gave similar results to ATE but was much slower regarding calculation time. The stereo blocks of each year were orientated separately. Although jointly adjusted image blocks would increase the relative accuracy between the blocks, it was not possible due to different visibilities of ground control points in different years. We want to demonstrate the workflow for future campaigns where a re-orientation of all existing blocks together is not feasible.

As this study focuses on snow depth mapping for wide scale applications, we set the spatial resolution of the derived DSM to 8*GSD (8*0.25 m), which results in significantly lower demand in CPU usage compared to a resolution at pixel level. Additionally we apply a 3*3 low pass filter to adapt the final products to the continuous nature of snow-covered areas.

In our research setup, single buildings and forest/scrub cannot be modeled with sufficient horizontal accuracy due to the limited spatial resolution of the input imagery. Slight differences in x,y positions of such objects in the summer and winter DSM would lead to big outliers in the snow depth product. Therefore all buildings and forest/scrub areas were masked out. For the detection of forest/scrub areas a combination of NDVI (Normalized Differenced Vegetation Index) and a canopy height layer was applied. With this approach, all visible vegetation in the winter images and vegetation higher than 1.5 m in the summer images were masked out. The detection of buildings (settlements) only from spectral or elevation information is not feasible since rock covered areas return an identical spectral signature as settlements and are prone to big outliers. Therefore we use the building layer from the Topographic Landscape Model (TLM) of the Swiss Federal Office of Topography. This step might not be necessary if the input imagery would have a higher spatial resolution (15 cm or better).

Large-scale imagery of a mountainous, snow covered landscapes show a maximal range of radiometric image information over short distance, which is highly demanding for image correlation processes. For this reason generating a complete DSM from one entire image strip is not expected to give optimal results for snow covered areas. As a response to this challenge we divided the test site in 809 tiles for which DSMs were calculated separately. Another well-known difficulty in steep mountain areas is a sub-optimal viewing angle or even occlusion in an image strip. Considering this difficulty, we calculated two DSMs for each tile, using the "most nadir" and the "second most nadir" - CIR image strips (near infrared, red, green) to increase the chance of a good image match for a given point on the ground. For the generation of the final DSM we calculated the mean slope for every processed DSM-tile. By selecting the DSM with the smaller mean slope for every given tile, big blunders caused by a not optimal viewing angle or occlusion could mostly be automatically eliminated. We used the described approach to process all DSMs.

The orientation of ADS80 image strips has to be considered as a critical point especially for winter images. All processing and evaluation efforts are worthless if there is a lack of accuracy in image orientation. Due to a small number of highly accurate reference points in remote areas and sometimes almost unrecognizable ground control points in snow covered, high alpine regions (e.g. east part of Dischma valley without any anthropogenic features) orientation quality shows certain limitations. For the mentioned areas, orientation during the post processing of image strips (software Leica xPro) could not be substantially improved, resulting in a final orientation accuracy of about 1 GSD. Well distributed artificial reference points measured at the ground with dGNSS could improve the orientation quality substantially but were not available for the winter 2012 imagery.

5 Results and validation

To quantify the accuracy of the digital photogrammetry products, we use the following measures recommended by Höhle and Höhle (2009) to compare elevation datasets from different sources:

a) The root mean square error

$$\mathbf{RMSE} = \sqrt{\frac{1}{n}\sum_{i=1}^{n} \Delta h_i^2} \quad (1)$$

this measure is often used and simple to calculate but very prone to outliers.

b) Normalized median absolute deviation

$$\mathbf{NMAD} = 1.4826\, median_j(|\Delta h_j - m_{\Delta h}|) \quad (2)$$

where Δh_j denotes the individual errors and $m_{\Delta h}$ is the median of the errors.

c) Additionally we use the empirical correlation coefficient

$$\mathbf{cor_e} = \frac{\sum(x-\bar{x})((y-\bar{y})}{\sqrt{\sum(x-\bar{x})^2 \sum(y-\bar{y})^2}} \quad (3)$$

to assess how well two snow depth measurements from different sources correlate.

To make the comparison of elevations in DEM products possible it is crucial that a coherent coordinate system is applied for all datasets. We use the swisstopo LV03 LN02 (CH1903) system with the elevation reference point at Repère Pierre du Niton H(RPN)=373.6 m a.s.l. in Geneva, Switzerland (swisstopo 2008).

5.1 Photogrammetric summer DSMs (DSM_{ADS})

Three DSM_{ADS} (winter 2012, summer 2010 and 2013) were processed for this study. For a quantification of the quality of the derived DSM_{ADS} we perform an accuracy assessment using a digital terrain model (DTM_{ALS} representing the bare ground without vegetation or buildings) acquired by an Airborne Laser Scanner ALS (Riegl LMS-Q240i) mounted on a helicopter in summer 2009 as a reference, assuming the changes in terrain to be negligible (which might not be true for areas prone to erosion and deposition). The average point density acquired was 2 – 3 points/m^2 from an average flight height of 300 m above ground. Airborne laser scanning is reported as very accurate method for DTM generation in various studies (e.g. Aguilar and Mills 2008 Höhle and Höhle 2009) also on snow (Deems et al. 2013) and in high alpine terrain (Bühler and Graf 2013). The quantification of the accuracy is described by the distributions of vertical deviations between the two datasets (886'000 points). Vegetation and buildings were excluded for the analysis.

The statistical measures in Table 1 show a good correspondence between the DTM_{ALS} and DSM_{ADS}. The RMSE value without outlier removal indicate the presence of big outliers. Since the mean values of the deviations with and without outlier removal differ only by 3 cm these big outliers are both, negative and positive. A detailed quality assessment on DSMs derived by ADS80 image strips in very steep and complex alpine terrain showed that the accuracy of photogrammetric DSMs decrease significantly in terrain steeper than 50°, explaining the occurrence of the above mentioned outliers (Bühler et al. 2012).

In Figure 3 on the right image correlation completeness in terms of correlated and interpolated points is shown for a section of testsite Wannengrat for winter 2012. Image matching completeness for the whole test site is given in Table 2 (Wannengrat and Dischma without buildings and vegetation). These results show the high matching success with the 12 bit imagery in particular over snow coverd areas.

5.2 Snow depth maps

The snow depth maps are calculated by subtracting the photogrammetric winter DSM from the summer DSM. The spatial resolution is 2 m as for the input DSMs. Because negative snow depths cannot occur values smaller than zero are set to “no data”. Consulting the input orthophotos of the winter data acquisitions allows identifying whether a certain area is snow free or not. Overall, 19.42% of all pixels are classified as trees and scrubs and 1.65% as buildings. From the remaining pixels 4.83 % were classified as ”no data”.

The generated snow depth maps (Fig. 4 and Fig. 5.) reveal a very high spatial variability of snow depth even within small distances. Snow depth can vary by more than 5 m within a few meters. Snow traps for wind-blown snow and deposits from past avalanche events are clearly visible. We identify the same snow trap features in the Wannengrat area, which were reported by Schirmer et al. (2011) measured in winter 2008. This indicates that snow traps and cornices are persistent over different winters due to dominant main wind directions. High snow depths due to avalanche deposits are persistent in tracks where avalanches occur several times each winter but are not where avalanches occur with return periods of more than one year.

The large area at the northern edge of the Dischma test site (Fig. 5) classified as “no data” is Lake Davos. This natural lake is used for power generation during winter and the surface level is lowered by up to 50 m. By subtracting the winter DSM from the summer DSM we get clearly negative values in this area, which are classified as outliers. The large outlier areas at the southern edge of the investigation area are the glaciers of the Grialetsch range. These small glaciers lost a significant part of their volume between summer 2013 (summer DSM) and winter 2012 (winter DSM) and their surface elevations were lowered (Zemp et al. 2006). Therefore highly positive values occur and are classify as outliers. Further outliers occur in very steep terrain (> 50°) because the footprint of the sensors is very small in such areas (Bühler et al. 2012), demonstrating the limitation of the proposed method for snow in rock faces. These areas are less relevant for most snow depth applications because little snow usually accumulates in very steep terrain (e.g. Fischer et al. 2011).

5.3 Snow depth validation using independent reference datasets

5.3.1 Differential Global Navigation Satellite System (dGNSS) measurements

A comparison of the ADS derived Winter 2012 DSM with 137 dGNSS points, describing elevations in m a. s. l. (top of the snow cover) results in a RMSE of 0.37 m and a NMAD of 0.28 m. With a mean of 0.21 m the ADS DSM models the surface of the snow cover systematically higher than dGNSS measurements. For the area Wannengrat in Figure 1a it can therefore be assumed, that snow cover thickness is overestimated using photogrammetric methods, mainly because of orientation inaccuracies. A bias introduced during the dGNSS survey could be caused by the penetration of the dGNSS device into the soft snow cover by a few cm`s which could explain some of the mean differences in elevation values between photogrammetry and dGNSS measurements.

5.3.2 Terrestrial Laser Scanning (TLS)

We compare the independently acquired TLS derived snow depth (TLS winter minus TLS summer) with the ADS derived snow depth (Figure 6a,b). In total we look at 55’272 pixels of 2 m resolution. It is hard to detect differences between the two snow depth products on first sight. All prominent snow features such as filled channels, cornices or blown out areas are clearly visible in both products. In the difference image between the two snow depth products, four regions with large deviations up to 2 m stand out (marked with black circles in Figure 6c). Three areas with significantly negative deviations (red, TLS higher than ADS) are located in small depressions. In these areas the incident angle of the laser beam is very flat resulting in lower accuracies. The ADS sensor is looking from nadir at these spots, producing more reliable snow depth values. On the ridge at the southern edge of the subset a large cornice was formed by wind during the winter (see Figur 2c in the background). This cornice is mapped with too large snow depth values by the ADS dataset because of the nadir-viewing angle. The TLS sensor is seeing the overhanging cornice from below producing better snow depth measurements than the ADS. However the correlation analysis for the two snow depth measurement methods results in cor_e = 0.94, the RMSE is 0.33 m and the NMAD 0.26 m. This proves the quality of the ADS snow depth measurements especially concerning the complex, representative terrain of this subset (mean slope angle of 27°, ranging from 0° to 81°, elevations ranging from 2332 m to 2639 m a.s.l.).

5.3.3 Hand-measure plots

The comparison of the snow depth values derived from the ADS80 DSMs to the manual plot measurements is given in Table 3. In three out of the 15 plots the snow depth exceeds the length of the avalanche probe (3.2 m) and the correct values could not be measured at all 25 points (measurements deeper than 3.2 m: plot1, 14; plot11, 5; plot 13, 5). The hand measurements could also be distorted by not plumb-vertical penetration of the snow cover (especially in deep snow packs), by thick ice layers in the snowpack, which cannot be penetrated by the avalanche probe, by rough bedrock or by inaccuracies of the positioning by dGNSS. Therefore we average the 25 single measurements and compare the mean and standard deviation of an entire plot to the ADS80 DSM based snow depth values (mean of all cells within the plot area).

The RMSE is 0.35 m for the mean snow depth and the standard deviation 0.13 m over all plots. The NMAD is 0.22 (mean) and 0.06 m (std). The correlation coefficient cor_e for the mean snow depth is 0.92 and 0.81 for the standard deviation. If we eliminate the three plots (1, 11 and 13), which contain unreliable measurements, the RMSE is reduced to 0.19 (mean) and 0.11 (std) and the NMAD to 0.18 m (mean) and 0.06 m (std). The correlation coefficients shift to 0.95 (mean) and 0.76 (std). The standard deviation is underestimated by the DSM_{ADS} derived snow depth values due to the smoothing effect of the 2 m pixel size. However these results indicate the feasibility of the proposed method for snow depth mapping.

5.3.4 Ground Penetrating Radar (GPR)

To allow comparison between GPR snow depth measurements and the ADS measurements, we assigned all individual 18 136 GPR point measurements to the 2 m × 2 m ADS raster, and calculated the mean of all GPR values within each cell, resulting in 1522 cells with GPR-based comparison data. The variability of the GPR snow depth within these cells amounted to between 0.1 and 0.3 m. Parts of the GPR data have been obtained close to taller vegetation such as trees and bushes. However, heavily affected measurements have been masked out before comparison, as ADS data cannot represent snow depth under forest canopy.

Comparing GPR to ADS data results in an overall RMSE of 0.43 m and an NMAD of 0.36 m. This is approx. 0.1 m worse compared to the reference data sets acquired at the Wannengrat area. The overall correlation coefficient between both data sets is 0.45 (Fig. 7a) only, note however that the GPR data set features a significantly lower range in snow depth when compared to the TLS data set (Fig. 6), mainly because it was acquired at the valley bottom. When analyzing different segments of the GPR dataset we find considerable differences. While the correlation is acceptable for individual GPR segments that feature large snow depth variability (Fig. 7b) it appears less favorable for GPR segments with a small variability in snow depth (Fig. 7c). By comparing the profiles of the snow depth values along the two segments N0. 1 and 5 (Fig. 7d,e) we find the ADS values to be too low over large parts of the transects. The agricultural zones at the Dischma valley bottom are covered by grass with a length of 0.1 to 0.5 m during summertime, when the ADS data was acquired. This explains partially why the ADS snow depth values are too low. In the profile No. 5 (Fig. 7d) the first 200 m of the segment is on meadow. The second part is on a road, running along a slope. While the GPR snow depth values remain quite constant, the ADS snow depth values show a large variability. While all GPR measurements are made strictly on the road the 2 by 2 m ADS pixels include adjacent areas on both sides of the road which could be nearly snow-free or covered by deep snow covers at the edge of the road. Another explanation for the worse accordance between GPR and ADS snow depth values might be the greater distance of the ADS sensor to the ground. While the Wannengrat reference data sets have been collected in an altitude of approximately 2400 m a.s.l., the valley ground of the Dischma, where the GPR data has been collected, has an elevation of approximately 1600 m a.s.l. This results in a coarser effective ground sampling distance (GSD) and therefore in a lower accuracy of the corresponding ADS data set. This finding indicates that spatial resolution of input imagery matters for the accuracy of the resulting snow depth estimates.

6 Discussion

Compared to airborne laser scanning the proposed method is expected to be slightly less accurate but more economic if large areas (> 100 km^2) have to be covered repeatedly. To assess the economic advantage of digital photogrammetry we requested quotations from three independent data providers offering digital surface models generated by airborne laser scanning and digital photogrammetry to cover the investigation area of this study (145 km^2). We asked for a GSD of 2 m for the final DSM and a vertical accuracy of approx. 30 cm (RMSE). Table 5 presents an overview on the answers we received. Digital photogrammetry is 40 - 50 % more economical than ALS in data acquisition, mainly because of the more efficient flight pattern resulting in reduced flight time for a given area. Data processing is 10 to 40% more economical resulting in a significant total price reduction of 25 to 37%. Now the successor sensor Leica ADS100 is available, incorporating almost twice as many detectors than the ADS80 sensor, resulting in a better spatial resolution for the same flying height above ground.

Digital photogrammetric DSMs can be generated using Unmanned Aerial Vehicle (UAV’s) flying close to the ground and producing higher spatial resolution imagery (Mancini et al., 2013) in the order of centimeters resulting in more accurate (better than 10 cm in vertical direction) and much more economic snow depth maps. However, the feasibility of UAVs in high alpine terrain has to be further investigated. Winged UAV's might not be stable enough under windy conditions, which are usually present in alpine terrain. Furthermore it might be difficult to find suitable starting and landing spots due to the rough terrain. UAV's with rotors are much more stable and can acquire data under windy conditions if the wind is not gusty. However they have very limited flight times due to high energy consumption and the batteries have to be changed very often (approx. every five minutes). UAV's with rotors are not yet able to efficiently cover areas larger then a few square kilometers in alpine conditions and the risk of crashing the UAV in rocky terrain is high.

Challenging for image correlation on snow-covered terrain are the big spectral differences of surface cover properties between bright snow-covered slopes and rocky terrain in shadow. If terrain properties change within short distances, the probability of big outliers or even complete failures of image matching rises. We modeled only 0.25 km^2 per step to decrease these differences within the correlated images. With this approach massive failure of image matching could mostly be averted. For some tiles, issues with big outliers remained, showing a certain limitation to the modeling of snow-covered areas with the used image correlation software. For future investigations the choice of more advanced image correlation algorithms like methods of the semi-global matching family has potential to solve part of this limitation. The modeling of steep slopes (>50°) using image-matching techniques is not accurate mainly due to the small footprint of the sensor (Bühler et al. 2012). But because snow accumulation is reduced in such steep slopes (Schweizer et al. 2008, Fischer et al. 2011), these areas are less important for applications in hydrology and avalanche science. The proposed methodology does not work in forested terrain or in regions covered by scrubs. Therefore these areas were masked out prior to the snow map calculation. This is not possible for areas with high grass in summer; therefore we clearly underestimate the snow depth with the ADS data in such areas (see Fig. 7d,e). In forested terrain ALS has a strong advantage compared to photogrammetry because the terrain surface can be measured between the trees if the forest cover is not too dense. The accuracy of final DSM products depends heavily on the image strip orientation quality. Here we faced two major limitations: a) we could gather only a small number of reference points, measured with high accuracy in x, y and z and b) in areas deeply covered by snow without anthropogenic signs visible, the recognition of clearly identifiable reference points is sometimes almost impossible. Therefore we see big potential to increase the quality of final products by collecting more accurately measured reference points and by signalizing reference points in remote parts of the covered area for upcoming data acquisition campaigns. But such fieldwork can be costly if several people have to be deployed in the field to cover large areas and different elevation levels in difficult terrain, reducing the economic advantage of photogrammetry.

7 Conclusions

The presented results demonstrate the potential of digital photogrammetry for catchment wide snow depth mapping. The extensive validation using independent datasets acquired simultaneously reveals an accuracy of approximately 30 cm (RMSE, NMAD), equivalent to ~1 GSD of the input images (Table 4). Due to the high radiometric resolution of the images (12bit) and the use of the near infrared band, the images were not saturated over bright, snow covered areas and information could be acquired even in cast shadow. The image correlations works even over very homogeneous areas. Table 2 reveals almost the same correlation success with winter images compared to summer images. The resulting snow depth maps visualize the high spatial variability of snow depth even within short distances of a few meters. Snow traps for wind-blown snow, cornices and deposits from past avalanche events can be identified easily by high snow depth values up to 15 m.

In this paper we applied six different methodologies to map snow depth in high alpine terrain. Table 6 lists the major strength and weaknesses of these methods based on the experience of the authors. However, which method should be applied in a specific case depends on many different factors and should be evaluated with care.

We plan to acquire similar datasets at the end of upcoming winters for inter-annual comparison of snow depth. This would also open the door for investigations on the representativeness of snow depth measurements at given points, for example at automated weather stations. Future comparisons between snow depth maps generated by LiDAR and digital photogrammetry will provide more detailed information on the specific strengths and weaknesses of the two methods.

Acknowledgements

The authors thank Leica Geosystems for the provision of the ADS80 datasets, the SLF field teams for helping with the reference data acquisition and the reviewers their constructive comments.

References

Aguilar, F. J. & Mills, J. P.: Accuracy assessment of lidar-derived digital elevation models. Photogrammetric Record, 23, 148-169, 2008.

Bavay, M.; Lehning, M.; Jonas, T. and Löwe, H.: Simulations of future snow cover and discharge in Alpine headwater catchments. Hydrological Processes, 23, 95-108, 2009.

Bründl, M., Etter, H.-J., Steiniger, M., Klingler, C., Rhyner, J. and Ammann, W.: IFKIS - a basis for managing avalanche risk in settlements and on roads in Switzerland. Natural Hazards and Earth System Sciences, 4, 257 – 262, 2004.

Buchroithner, M. F.: Problems of mountain hazard mapping using spaceborne remote sensing techniques. Advances in Space Research, 15, 57-66, 1995.

Bühler, Y.; Meier, L; Ginzler, C. Potential of Operational High Spatial Resolution Near-Infrared Remote Sensing Instruments for Snow Surface Type Mapping. IEEE Geoscience and Remote Sensing Letters, 12 (4), 1–5, DOI: 10.1109/LGRS.2014.2363237. 2015.

Bühler, Y.; Hüni, A.; Christen, M.; Meister, R. and Kellenberger, T.: Automated detection and mapping of avalanche deposits using airborne optical remote sensing data. Cold Regions Science and Technology, 57, 99–106, 2009.

Bühler, Y., Marty, M. and Ginzler, C.: High Resolution DEM Generation in High-Alpine Terrain Using Airborne Remote Sensing Techniques. Transactions in GIS. 2012, 16 (5), 635 – 647, 2012.

Bühler, Y and Graf, C.: Sediment transfer mapping in a high-alpine catchment using airborne LiDAR. In: Graf, C. (Red.) Mattertal - ein Tal in Bewegung. Publikation zur Jahrestagung der Schweizerischen Geomorphologischen Gesellschaft 29. Juni - 1. Juli 2011, St. Niklaus. Birmensdorf, Eidg. Forschungsanstalt WSL. 113-124, 2013.

Chang, A.; Foster, J.; Hall, D.; Rango, A. and Hartline, B.: Snow water equivalent estimation by microwave radiometry. Cold Regions Science and Technology, 5, 259-267, 1982.

Cline, D.W.: Measuring alpine snow depths by digital photogrammetry: Part 1. conjugate point iden- tification, Proceedings of the Eastern Snow Conference, Quebec City, 1993.

Cline, D.W.: Digital Photogrammetric Determination Of Alpine Snowpack Distribution For Hydrologic Modeling, Proceedings of the Western Snow Conference, Colorado State University, CO, USA, 1994.

Deems, J.; Painter, T. and Finnegan, D.: Lidar measurement of snow depth: A review. Journal of Glaciology, 59, 467-479, 2013.

Dietz, A.; Kuenzer, C.; Gessner, U. and Dech, S.: Remote sensing of snow - a review of available methods. International Journal of Remote Sensing, 33, 4094-4134, 2012.

Dozier, J.: Snow reflectance from landsat-4 thematic mapper. IEEE Transactions on Geoscience and Remote Sensing, GE-22, 323-328, 1984.

Dozier, J.: Spectral signature of alpine snow cover from the Landsat thematic mapper. Remote Sensing of Environment, 28, 9-22, 1989.

Dozier, J.; Green, R. O.; Nolin, A. W. and Painter, T. H.: Interpretation of snow properties from imaging spectrometry. Remote Sensing of Environment, 113, 25-37, 2009.

Egli, L.: Spatial variability of new snow amounts derived from a dense network of Alpine automatic stations. Annals of Glaciology. 49, 51-55, 2008.

Egli, L.: Spatial variability of seasonal snow cover at different scales in the Swiss Alps. Diss. ETH. No 19658, 2011.

Egli, L., Jonas, T. Grünewlad T., Schirmer T. and Burlando, P.: Dynamics of snow ablation in a small Alpine catchment observed by repeated terrestrial laser scans. Hydrological Processes, doi 10.1002/hyp.8244, 2011.

Elder, K., Dozier, J. and Michaelsen, J.: Snow accumulation and distribution in an alpine watershed. Water Resources Research. 27, 1541-1552, 1991.

Elsasser, H. and Bürki, R.: Climate change as a threat to tourism in the Alps. Climate Research. 20, 253-257, 2002.

Farinotti, D., Usselmann, S., Huss, M., Bauder, A. and Funk, M.: Runoff evolution in the Swiss Alps: Projections for selected high-alpine catchments based on ENSEMBLES scenarios. Hydrological Processes. 26, 1909-1924, 2012.

Fily, M.; Bourdelles, B.; Dedieu, J. P. and Sergent, C. : Comparison of in situ and Landsat Thematic Mapper derived snow grain characteristics in the Alps. Remote Sensing of Environment, 59, 452-460, 1997.

Fischer, L.; Eisenbeiss, H.; Kaab, A.; Huggel, C. and Haeberli, W.: Monitoring Topographic Changes in a Periglacial High-mountain Face using High-resolution DTMs, Monte Rosa East Face, Italian Alps. Permafrost and Periglacial Processes, 22, 140-152, 2011.

Foppa, N., Stoffel, A. and Meister, R.: Synergy of in situ and space borne observation for snow depth mapping in the Swiss Alps. International Journal of Applied Earth Observation and Geoinformation. 9, 294-310, 2007.

Frei, A., Tedesco, M., Lee, S., Foster, J., Hall, D. K., Kelly, R. and Robinson, D. A.: A review of global satellite-derived snow products. Advances in Space Research, Oceanography, Cryosphere and Freshwater Flux to the Ocean, 50, 1007-1029, 2012.

Grünewald, T., Schirmer, M., Mott, R. and Lehning, M.: Spatial and temporal variability of snow depth and ablation rates in a small mountain catchment. Cryosphere. 4, 215-225, 2010.

Grünewald, T., and Lehning, M.: Are flat-field snow depth measurements representative? A comparison of selected index sites with areal snow depth measurements at the small catchment scale, Hydrological Processes, doi:10.1002/hyp.10295, 2014

Hall, D. K. and Martinec, J.: Remote Sensing of Ice and Snow. Chapman and Hall Ltd., London. ISBN 0 421 25910, 189pp., 1985.

Hall, D., Riggs, G., Salomonson, V., DiGirolamo, N. and Bayr, K.: MODIS snow-cover products. Remote Sensing of Environment, 83, 181-194, 2002.

Höhle, J. and Höhle, M.: Accuracy assessment of digital elevation models by means of robust statistical methods. ISPRS Journal of Photogrammetry & Remote Sensing, Vol. 64, 398-406, 2009.

Jonas, T., Marty, C. and Magnusson, J.: Estimating the snow water equivalent from snow depth measurements in the Swiss Alps. Journal of Hydrology, 378, 161-167, doi:10.1016/j.jhydrol.2009.09.021, 2010.

Koetz, B.; Arino, O.; Poulianen, J. & Bojkov, B.: GlobSnow - A new contribution to global snow monitoring services. European Space Agency, (Special Publication) ESA SP, 2008.

Kraus, K.: Photogrammetrie. Walter de Gruyter GmbH, Berlin, 7, 516 pp., 2004.

Ledwith, M. and Lunden, B.: Digital photogrammetry for air-photo-based construction of a digital elevation model over snow-covered areas - Blamannsisen, Norway. Norsk Geografisk Tidsskrift - Norwegian Journal of Geography, 55(4): 267-273, 2001.

Lee, C.Y., Jones, S.D., Bellman, C.J. and Buxton, L.: DEM creation of a snow covered surface using digital aerial photography. The International Archives of the Photogrammetry, Remote Sensing and Spatial Information Sciences, 37, 2008.

Lehning, M., Löwe, H., Ryser, M. and Raderschall, N.: Inhomogeneous precipitation distribution and snow transport in steep terrain. Water Resources Research. 44 (7), W07404, 2008.

Lopez-Moreno, J. and Nogues-Bravo, D.: Interpolating local snow depth data: An evaluation of methods. Hydrological Processes, 20, 2217-2232, 2006.

Mancini, F.; Dubbini, M.; Gattelli, M.; Stecchi, F.; Fabbri, S. & Gabbianelli, G.: Using unmanned aerial vehicles (UAV) for high-resolution reconstruction of topography: The structure from motion approach on coastal environments. Remote Sensing, 5, 6880-6898, 2013.

Melvold, K. and Skaugen, T.: Multiscale spatial variability of lidar-derived and modeled snow depth on Hardangervidda, Norway. Annals of Glaciology, 54, 273-281, 2013.

Nolin, A. W. and Dozier, J.: Estimating snow grain size using AVIRIS data. Remote Sensing of Environment, 44, 231-238, 1993.

Nolin, A.: Recent advances in remote sensing of seasonal snow. Journal of Glaciology, 56, 1141-1150, 2011.

Nöthiger, C. and Elsasser, H.: Natural hazards and tourism: New findings on the European Alps. Mountain Research and Development, 24, 24-27, 2004.

Painter, T. H., Roberts, D. A., Green, R. O. and Dozier, J.: The Effect of Grain Size on Spectral Mixture Analysis of Snow-Covered Area from AVIRIS Data. Remote Sensing of Environment, 65, 320-332, 1996.

Prokop, A.: Assessing the applicability of terrestrial laser scanning for spatial snow depth measurements. Cold Regions Science and Technology. 54, 155-163, 2008.

Pulliainen, J.: Mapping of snow water equivalent and snow depth in boreal and sub-arctic zones by assimilating space-borne microwave radiometer data and ground-based observations. Remote Sensing of Environment, 101, 257-269, 2006.

Rango, A. and Itten, K. I.: Satellite Potentials in Snowcover Monitoring and Runoff Prediciton. Nordic Hydrology, 7, 209 – 230, 1976.

Rixen, C., Teich, M., Lardelli, C., Gallati, D., Pohl, M., Pütz, M. and Bebi, P.: Winter tourism and climate change in the Alps: An assessment of resource consumption, snow reliability, and future snowmaking potential. Mountain Research and Development, 31,229-236, 2011.

Rott, H.: Synthetic aperture radar capabilities for snow and glacier monitoring Advances in Space Research, 4, 241-246, 1984.

Sandau, R. (Ed.): Digital Airborne Camera. Springer, The Netherlands, 2012.

Sandmeier, J.: ReflexW software package. http://www.sandmeier-geo.de/reflexw.html, 2013.

Schanda, E.; Matzler, C. and Kunzi, K.: Microwave remote sensing of snow cover International Journal of Remote Sensing, 4, 149–158, 1983.

Schirmer, M., Wirz, V., Clifton, A., and Lehning, M.: Persistence in intra-annual snow depth distribution: 1 measurements and topographic control, Water Resources Research, 47, W09516, doi:10.1029/2010wr009426, 2011.

Schweizer, J.; Jamieson, J. B. and Schneebeli, M.: Snow avalanche formation. Reviews of Geophysics, 41 (4), 2-25, 2003.

Schweizer, J., Kronholm, K., Jamieson, J. B. and Birkeland, K. W.: Review of spatial variability of snowpack properties and its importance for avalanche formation. Cold Regions Science and Technology, 51, 253-272, 2008.

Shi, J. and Dozier, J.: Estimation of snow water equivalence using SIR-C/X-SAR. II. Inferring snow depth and particle size. IEEE Transactions on Geoscience and Remote Sensing, 38, 2475-2488, 2000.

Smith, F., Cooper, C. and Chapman, E.: Measuring Snow Depths by Aerial Photography. Proceed- ings of the Western Snow Conference, 1967.

Swisstopo: Formeln und Konstanten für die Berechnung der Schweizerischen schiefachsigen Zylinderprojektion und der Transformation zwischen Koordinaten–systemen. Bundesamt für Landestopographie swisstopo, 2008.

Ulaby, F. and Stiles, W.: The active and passive microwave response to snow parameters, 2, Water equivalent of dry snow. Journal of Geophysical Research, 85, 1045–1049, 1980.

Wipf, S., Stoeckli, V. and Bebi, P.: Winter climate change in alpine tundra: Plant responses to changes in snow depth and snowmelt timing. Climatic Change. 94, 105-12, 2009.

Zemp, M., Haeberli, W., Hoelzle, M. and Paul, F.: Alpine glaciers to disappear within decades? Geophysical Research Letters, 33 (13), L13504, 2006.

Zhang, B. and Miller, S. (). Adaptive automatic terrain extraction. Proc. SPIE 3072, Integrating Photogrammetric Techniques with Scene Analysis and Machine Vision III, 27. doi_10.1117/12.281065, 1997.

Table 1. Statistical accuracy measures of error distributions (DSM_{ADS} – DTM_{ALS}) for 886’000 points in the test site Wannengrat (* outlier removal: ≥μ±3* RMSE).

μ	RMSE	μ*	RMSE*	Median	NMAD
0.19	0.9	0.16	0.33	0.16	0.24

Table 2. Correlated vs. interpolated terrain points in summer and winter DSM over the entire test site.

	correlated [n]	interpolated [n]	total [n]	correlated [%]
summer 2010	28’524’154	1’533’418	30’057’572	94.6
winter 2012	28’592’370	1’710’205	30’302’575	94.4

Table 3. ADS80 DSM derived snow depth values (4 by 4 pixels) compared to the hand measured snow depth values (5 by 5 single measurements) for the 15 plots. Plots where at least one measurement did not reach the ground are displayed in grey.

	min	max	mean	std	min ADS	max ADS	mean ADS	std ADS	Δ mean	Δ std
Plot 1	1.80	3.10	2.81	0.42	1.68	3.41	2.56	0.55	0.25	-0.13
Plot 2	0.85	2.50	1.43	0.53	0.52	2.16	1.25	0.52	0.18	0.01
Plot 3	1.20	1.75	1.43	0.16	0.90	1.72	1.14	0.15	0.29	0.01
Plot 4	0.35	0.90	0.50	0.15	0.30	0.59	0.43	0.09	0.07	0.06
Plot 5	0.55	1.75	1.01	0.34	0.04	1.84	0.79	0.53	0.22	-0.19
Plot 6	0.75	1.75	1.19	0.29	1.12	1.93	1.48	0.25	-0.29	0.04
Plot 7	1.35	2.90	2.32	0.47	1.98	2.69	2.34	0.21	-0.02	0.26
Plot 8	1.85	2.80	2.33	0.25	2.13	2.81	2.37	0.17	-0.04	0.08
Plot 9	1.40	2.20	1.71	0.23	1.43	2.04	1.69	0.17	0.02	0.06
Plot 10	0.55	2.35	1.34	0.56	0.77	2.14	1.40	0.38	-0.06	0.18
Plot 11	0.65	3.10	2.28	0.67	0.56	2.65	1.93	0.85	0.35	-0.18
Plot 12	0.15	0.35	0.22	0.06	0.06	0.24	0.14	0.05	0.08	0.01
Plot 13	2.30	3.10	2.59	0.33	2.89	0.49	3.71	0.49	-1.12	-0.16
Plot 14	0.70	2.00	1.37	0.41	0.43	1.62	1.12	0.32	0.25	0.09
Plot 15	0.35	1.60	0.97	0.33	0.75	1.81	1.33	0.27	-0.36	0.06

Table 4. Overview on the accuracy measures calculated from the different reference datasets.

Reference dataset	N° of observations	RMSE	NAMD	cor_e
ALS (summer surface)	886’000	0.33	0.24	-
dGNSS (winter surface)	137	0.37	0.28	-
Hand plots (snow depth)	12	0.19	0.18	0.95
TLS (snow depth)	55’272	0.33	0.26	0.94
GPR (snow depth)	1522	0.43	0.37	0.45

Table 5. Price ranges in thousand Swiss Franks (kCHF) and relative differences derived from quotations of three independent data providers. We asked to cover the investigation area of this paper (145 km^2) with airborne laser scanning (ALS) and digital photogrammetry with a spatial resolution of 2 m and a vertical accuracy of approx. 30 cm**.**

	Data acquisition	Data processing	Total
ALS	25 - 40 kCHF	25 - 40 kCHF	50 - 80 kCHF
Photogrammetry	12 - 24 kCHF	18 - 36 kCHF	30 - 60 kCHF
Relative Difference	40 – 52%	10 – 44%	25 – 37%

Table 6. Overview on the most important strength and weaknesses of the applied methods for **large-scale** snow depth mapping in high alpine terrain based on the experiences gained through this investigation.

Method	Strength	Weaknesses
Airborne Laser Scanning (ALS)	• Large coverage • Fast measurements • Spatially continuous • High precision • Nadir view	• Expensive • Costly data processing • Need for an airplane • Expensive device
Airborne Photogrammetry	• Very large coverage • Fast measurements • Spatially continuous • Many devices in use • Nadir view	• Limited precision • Costly data processing • Need for an airplane • Expensive device
Terrestrial Laser Scanning (TLS)	• Intermediate coverage • Spatially continuous • High precision • Suitable for steep slopes (> 50°)	• Oblique view • Need for being in the field • Costly data processing • Expensive device
Ground Penetrating Radar (GPR)	• High precision • Direct snow depth measurement	• Limited coverage • Transect measurements • Extreme terrain inaccessible • Need for being in the field • Expensive device
Hand plots	• Most economic method • Direct snow depth measurement • No special devices necessary	• Very limited coverage • Point measurements • Extreme terrain inaccessible • Need for being in the field

	• Possible in forested areas	
Differential Global Navigation Satellite System (dGNSS)	• High precision	• Very limited coverage • Point measurements • Extreme terrain inaccessible • Need for being in the field • Expensive device

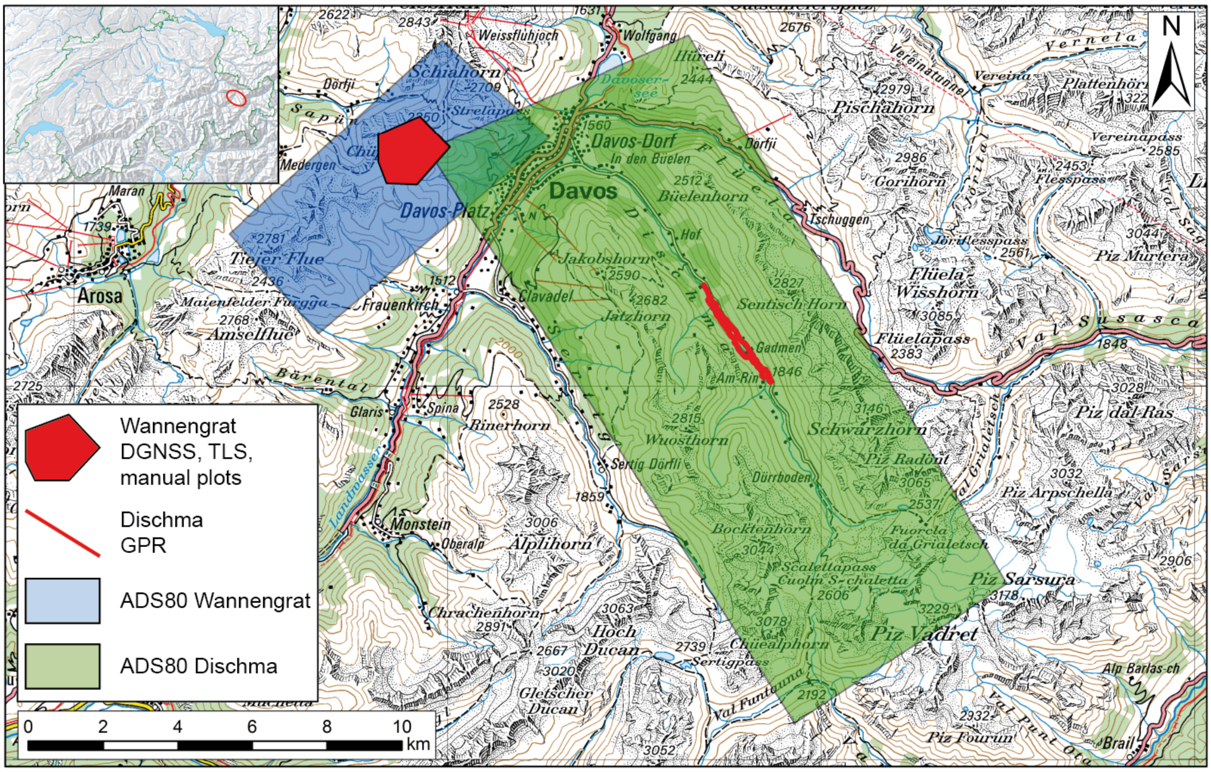

Figure 1. ADS80 data coverage and locations of the applied reference data sets at Wannengrat and in the Dischma valley close to Davos, Switzerland. Pixmap ©2014 swisstopo (5704 000 000).

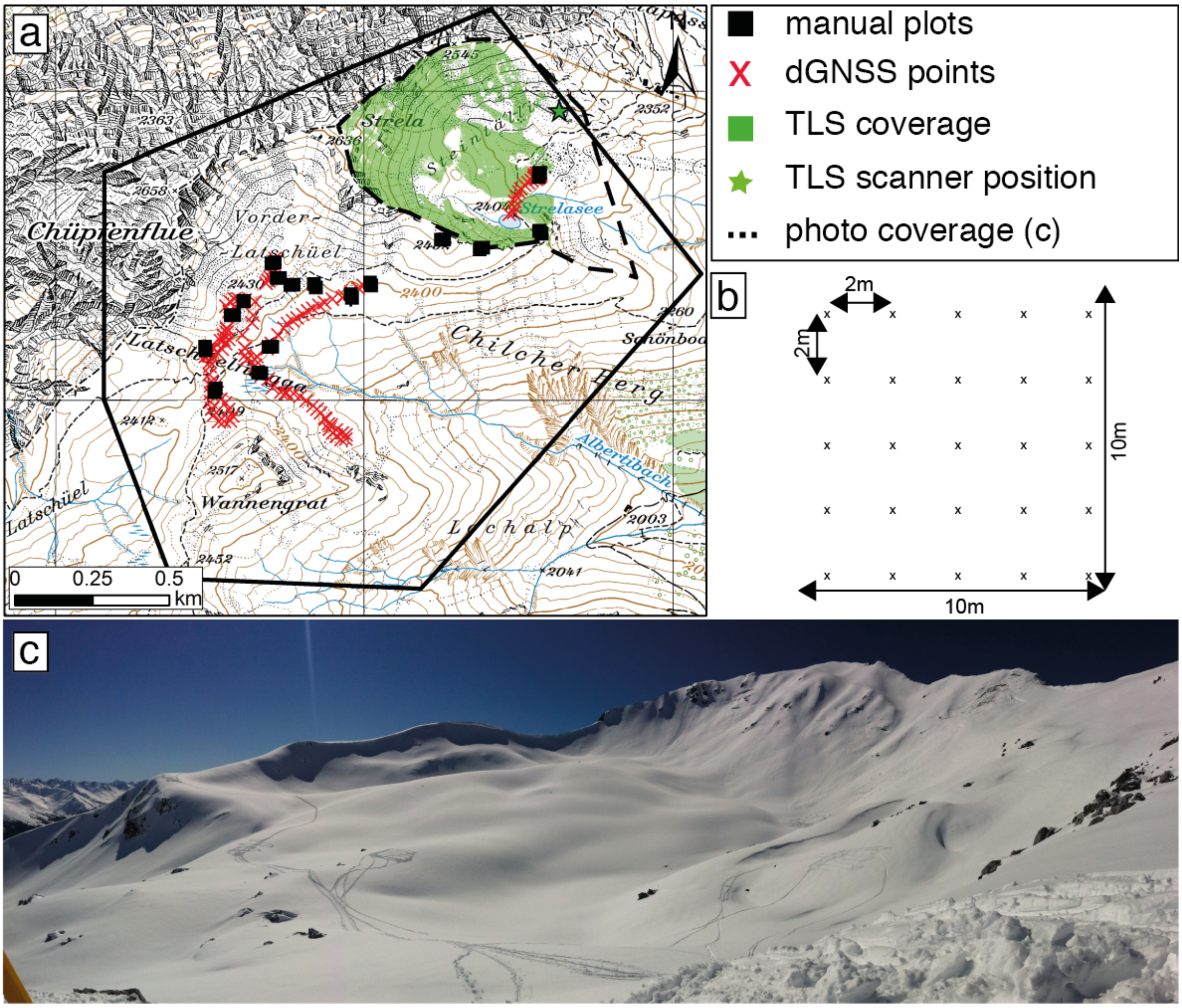

Figure 2. **Map of the locations of the plots measured by hand, the dGNSS measurements, the TLS coverage and the coverage of the panorama photograph (a); applied sampling strategy for the manual plots (b); panorama photograph of the Wannengrat test site (c). Pixmap ©2014 swisstopo (5704 000 000).**

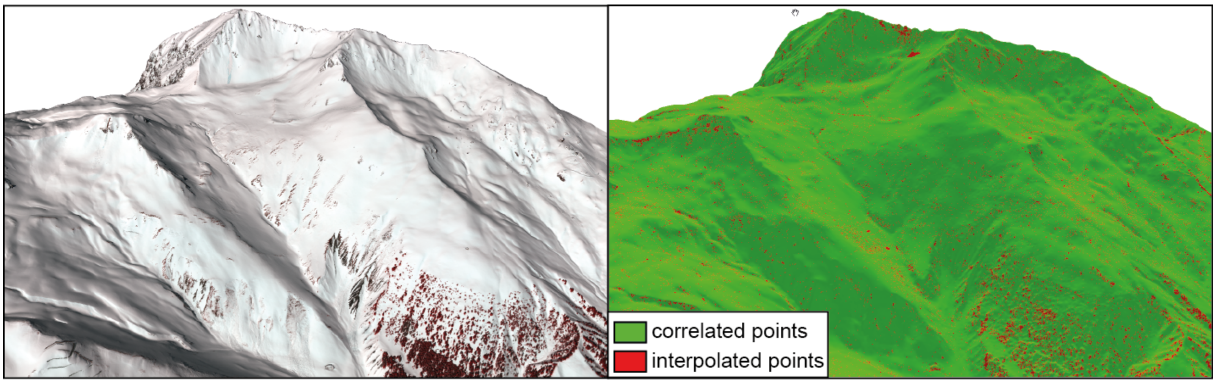

Figure 3. Spatial distribution of image correlation success in a section of the test site Wannengrat. Visible in the right picture are interpolated points (red) mainly in very steep terrain (>50°), on vegetation and anthropogenic features (e.g. ski lift).

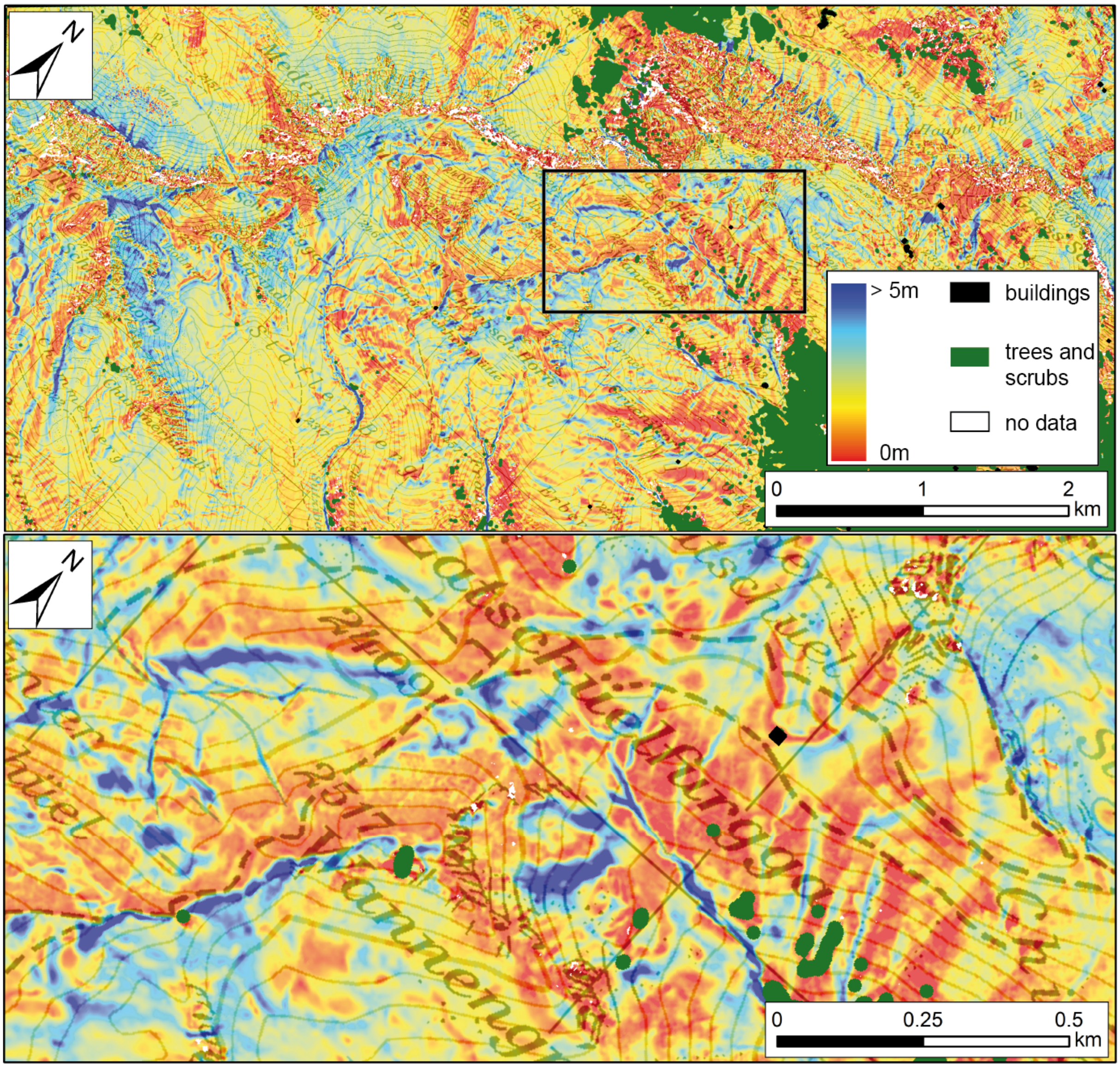

Figure 4. Snow depth map of the entire Wannengrat area (top, see Fig 1. for orientation) and a close up view from area where the reference data was acquired (bottom). Traps for wind-blown snow, cornices and deposits from past avalanche events can be identified by the highest snow depth values.

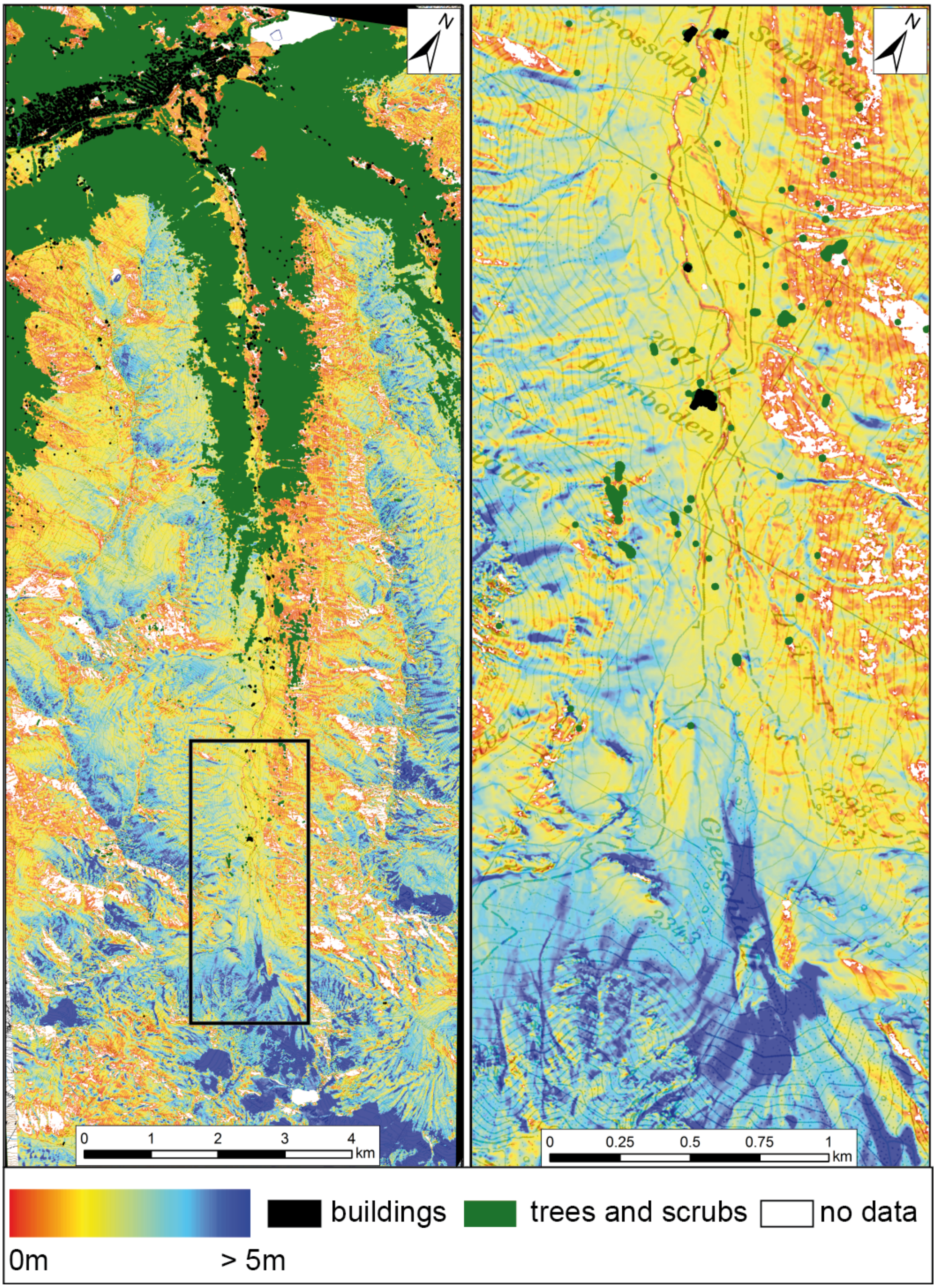

Figure 5. Snow depth map of the entire Dischma area (left, see Fig 1. for orientation) and a close up view (right) from area indicated by the black box.

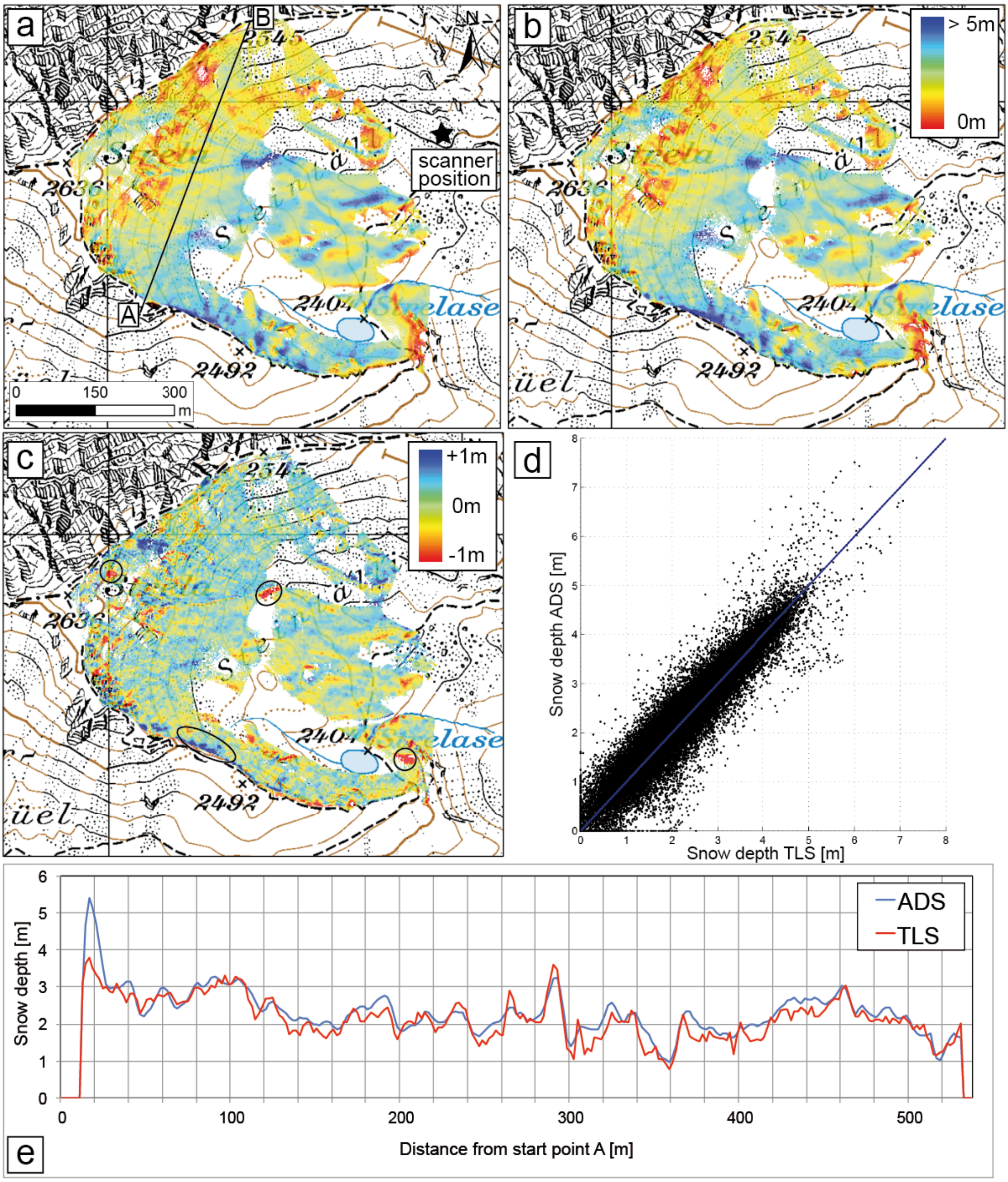

Figure 6. TLS derived snow depth **(a)**, ADS derived snow depth **(b)**, difference ADS minus TLS **(c)** scatter plot of the two different snow depth measurements **(d)** ($cor_e = 0.94$) and TLS as well as ADS snow depth values along a transect (depicted in **(a)**) from point A to point B **(e)**

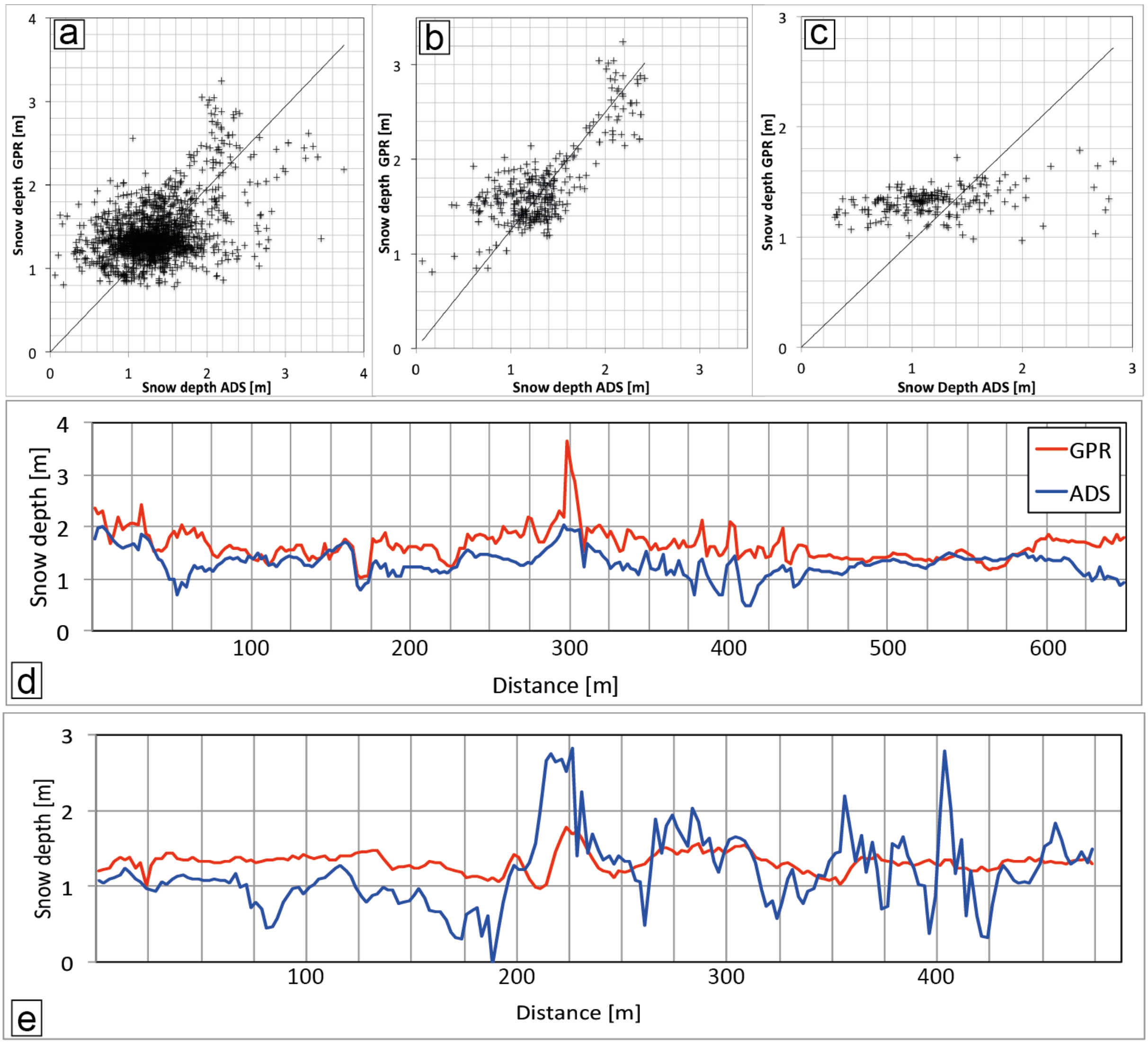

Figure 7. Correlation of the ADS snow depth to the GPR snow depth for all 1522 points (a, $cor_e = 0.45$), segment N° 1 with 296 points and a larger value range (b, $cor_e = 0.77$) and segments N° 5 with 191 points and a low value range in the GPR data (c, $cor_e = 0.34$).